Research Article | Vol. 27, No. 2 | 21 Jan 2019 | OPTICS EXPRESS 827
Optics EXPRESS

Holographic waveguides in photopolymers

R. Fernández,[1] S. Bleda,[1] S. Gallego,[1,*] C. Neipp,[1] A. Márquez,[1] Y. Tomita,[2] I. Pascual,[1] and A. Beléndez[1]

[1]*Universitario de Física Aplicada a las Ciencias y las Tecnologías, Universidad de Alicante, Apartado 99, 03080 Alicante, Spain*
[2]*Departament of Engineering Science, University of Electro-Communications, 1-5-1 Chofugaoka, Chofu, Tokyo 182-8585, Japan*
**sergi.gallego@ua.es*

Abstract: The possibilities that offer the holographic optical elements for photovoltaic and "see through display" applications open new windows for holographic recording materials. In this sense, some specific characteristics are required for each particular application. Waveguides are one of the key elements for these applications. Photopolymers are one of the most competitive candidates for waveguide fabrication. In this work, we evaluate the performance of one example from each of three families of photopolymer material in fabrication of a 633nm waveguide. Firstly, polyvinyl alcohol acrylamide, PVA/AA, the second one, a nanoparticle-thiol-ene, NPC, and on the last place a penta/hexa-acrylate based polymer with dispersed nematic liquid crystal molecules, PDLC. We study the critical role of the material and in particular, spatial resolution for this application.

1. Introduction

Dry photopolymeric materials are holographic recording media with important characteristics such as low price, self-processing capability and a high versatility. These characteristics, among many others, offer significant advantages over conventional wet-type recording materials [1]. Their wide potential in photonics and communications have been long and extensively studied. There are interesting applications and development in diffractive optics [2,3], optical communications [4], photonic crystal [5], holographic data storage [6], sensors [7], solar concentrators [8], wearable eyeglasses [9] and waveguides [10,11]. This last application can be designed as a tool or supporting technology for more complicated displays, such as photovoltaic concentrators or see-through eyeglasses [12]. For each technology, the recording material has to be optimized for specific requirements, such as shrinkage, refractive index modulation, monomer diffusion, recording sensitivity, thickness, storage dynamic range, polymerization degree, etc [13]. Therefore, before using a photopolymer in a certain application, it is important to carry out material optimization and, when it is possible, to model the material's behavior. In the case of waveguides there are different ways to fabricate them with holographic recording materials and, in particular, photopolymers. Previously, waveguides have been fabricated using different holographic architectures [14–16]. Additionally, waveguides can be self-written in these materials [10,11]. The last possibility is the fabrication by holographic transmission architecture [17]. In this work, we focus our attention in this last possibility, firstly explored in [17]. The purpose was to use a photopolymer grating to diffract 633nm light (at normal incidence) at such an angle that it would be guided (trapped) within the glass; this was achieved by recording a volume holographic optical element at a shorter wavelength of 532nm.

For this particular application, the holographic photopolymer material should be adequately designed and optimized. Two characteristics of this holographic recording material are critical for this kind of waveguides. On the first place, the spatial response of the material must be evaluated, because spatial frequencies higher than 1500 lines/mm are required for this purpose [17]. Nevertheless, the size of the polymer chains limits the

#345356 https://doi.org/10.1364/OE.27.000827
Journal © 2019 Received 10 Sep 2018; revised 13 Nov 2018; accepted 13 Nov 2018; published 11 Jan 2019

Optics EXPRESS

attainable refractive index modulation at high spatial frequencies. This effect is well explained by the non-local model [18] for binder-based all-organic photopolymer materials. In order to overcome it, some authors propose the inclusion of chain-transfer agents to reduce the average length of the polymer chains [19], in particular for reflection-type holographic gratings, where the spatial frequencies are higher than 3000 lines/mm. On the second place, an effect of the slanting of the fringes on the grating fidelity must be taken into account. For the fabrication of diffraction gratings to be used in holographic waveguides, the material must be able to adequately record highly slanted gratings. This kind of holographic optical elements, HOEs, are highly affected by the shrinkage process, which deforms the grating structure, and also the Bragg condition, resulting in a reduction in the refractive index modulation [20].

In this paper, we investigate the responses for different spatial frequency and slanted gratings of three different photopolymers for recording such waveguides: polyvinyl-acrylamide based photopolymer [20], PVA/AA, with a functionality slightly higher than one, a nanoparticle-(thiol-ene) polymer composite dispersed with SiO_2 nanoparticles [21–23] and average functionality higher than two, NPC, and a photopolymer with dispersed liquid crystal molecules [24], with average functionality higher than five, PDLC. This investigation is initially carried out recording symmetric sinusoidal gratings. Additionally, we propose three different experimental recording architectures for all the three photopolymer materials and an additional geometry adapted for holographic recording materials with low spatial resolution. The first one is similar to the analyzed in [17], where the spatial frequency is around 1700 lines/mm and the tilt angle of the grating vector with the light propagation inside the material is 69°. We also consider two other recording setup schemes: one with a change in the incident angle of the reference beam to reduce the grating's tilt angle, although it requires increasing the grating's spatial frequency. The other is the use of a lower spatial frequency,1000 lines/mm, which requires, however, a further grating tilt angle.

2. Theoretical background

The idea behind the transmission holographic waveguide is basically explained in Fig. 1. The task of the diffraction grating is to couple the energy of the incident beam, whose propagation vector is denoted by $\boldsymbol{\rho}$, to the diffracted beam, whose propagation vector is denoted by $\boldsymbol{\sigma}$. The diffracted beam must be deflected so that the angle formed with respect to the normal of the glass substrate be higher than the critical angle, θ_c, (for the interface glass-air) in order to accomplish total internal reflection.

As we mentioned before, three different possible recording geometries are analyzed in this paper to trap the light inside the layer. It can be achieved with more or less spatial frequency and fringes with different tilt angles. The key of the proposed waveguide is that the object beam, recorded by 532 nm, impinges with an angle such that when reconstructed by He-Ne, 632.8 nm, it gives a propagation angle inside the layer higher than 41.5°, to obtain total reflection inside the substrate and guide the light.

Optics EXPRESS

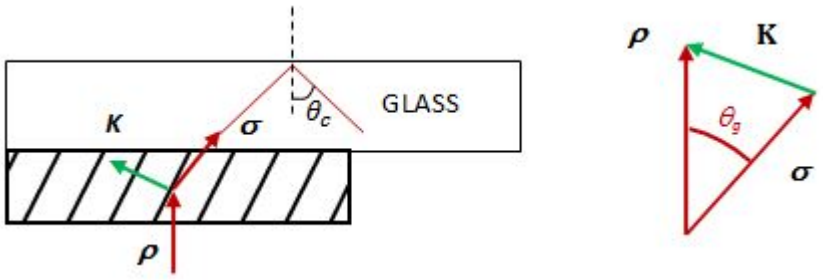

Fig. 1. - Grating coupler. Slanted Grating recorded in Photopolymer (n_1 = 1.49) over glass substrate (n_2 = 1.51) and the graphical relation between the diffraction, transmitted and grating vectors.

It is worth noting that the grating vector, **K**, can be obtained easily from the two interfering wave vectors, **ρ** and **σ**, as follows:

$$\boldsymbol{\sigma} - \boldsymbol{\rho} = \mathbf{K} \tag{1}$$

Where $|\boldsymbol{K}| = \frac{2\pi}{\Lambda}$ and $|\boldsymbol{\rho}| = |\boldsymbol{\sigma}| = n\frac{2\pi}{\lambda}$, Λ is the grating period, λ is the wavelength and n is the average refractive index of the sample. For the materials analyzed in this work, n = 1.49 and the glass used as substrate has n = 1.51, the dispersion of the refractive indices for red and green is negligible in this case. We design our experiment to obtain an angle propagation of θ = 41.7 °, larger than the θ_c.

The geometries of the gratings analyzed in this paper are shown in Fig. 2, where the Ewald's sphere is presented. Initially, the light propagation is along the Z positive direction. The radius of this sphere is equal to $\frac{2\pi}{\lambda}n$, all the angles are inside the material, β_1 is the angle of the object beam with the normal and β_2 is the angle of the reference beam with the normal. The upper indices "g" o "r" are related to the wavelengths, green, 532 nm, for the recording of the hologram and red, 633 nm, for the readout respectively. Geometry A has a spatial frequency of 1700 lines/mm and was designed to guide red light with normal incidence. Geometry B has a spatial frequency of 2000 lines/mm and less inclination of the grating fringes, was designed for materials with problems related to slanted gratings and good spatial resolution. The angle of the grating vector **K** with the normal in geometry A is 69.15 ° and for geometry B is 72.03°. It is important to remark that for unslanted gratings the angle of **K** with the normal is 90°. The variation between geometries A and B can seem to be not so high, but we have measured some important differences in the results. In any case, the main advantage of the option A is the normal incidence for the reconstruction at the wavelength that we want to guide in the material, in this case red light, because normal incidence is easy to find in experimental conditions. Attending to the spatial resolution limitation found for NPC photopolymer we proposed recording geometry C where the angle of **K** is 60.77°, but the spatial frequency is 1000 lines/mm. The angles are marked with prime for geometry B and double prime for geometry C.

Optics EXPRESS

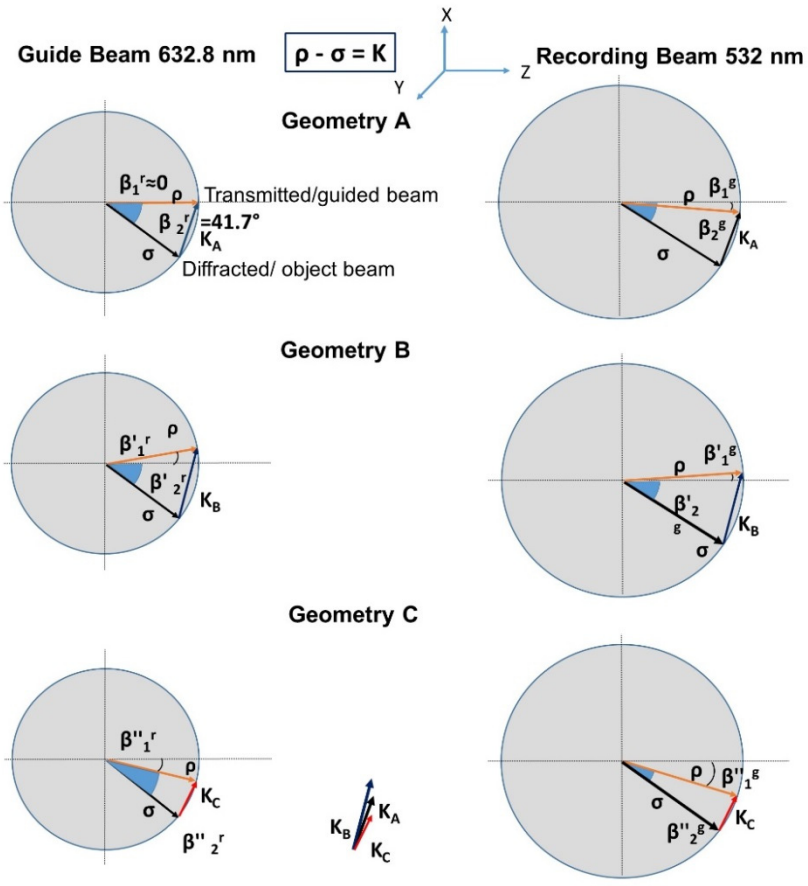

Fig. 2. Ewald's sphere and recording (right) and read out (left) geometries for three slanted gratings. Geometry A: designed for normal incidence of red light. Geometry B: less inclination of the grating fringes. Geometry C: higher inclination of the grating fringes. In the middle down graphical comparison of the three gratings vectors.

3. Experimental set up

To be sure that the spatial resolution is enough to store the holographic wave guides we use the recording of symmetrical gratings, the initial beam, with 2.4 mW/cm^2 for all the experiments, was split in two identical beams and for the waveguide recording, geometries A and B, the beam closer to the normal has an intensity of 0.7 mW/cm^2 whereas the most tilted beam has 1.7 mW/cm^2 in order to obtain an intensity beam relation near 1:1 in the interference zone on the material. For geometry C, the intensities are 0.6 mW/cm^2 and 1.8 mW/cm^2 respectively. All the lasers used in our experiments have s polarization.

It should be noted that the DE from a waveguide structure used in our experiment cannot be directly measured because the diffracted beam is trapped inside the glass substrate of the sample at a diffraction angle larger than the critical angle at the boundary between the glass substrate and the air. The diffraction beam goes out from the edge of the glass substrate. For this reason, we evaluated the transmission efficiency (TE), defined as the ratio of the transmitted power to the incident one, of our holographic optical elements (HOE), without Fresnel correction at s polarization. We found that the sum of TE and DE in our experiment

Optics EXPRESS

was close to 0.9. In this way angular responses of the waveguide were measured using transmitted beam, to avoid the movement of the detector to capture the diffracted beam.

PVA/AA based photopolymer was widely used for various optical applications [25–27]. The particular chemical composition used in our experiments can be described as follows: polyvinylalcohol, 25 ml (8% weight/volume), as the binder to give physical consistence to the layer, and acrylamide as main monomer, 0.84g, with functionality one. The crosslinker added to the solution is N, N'-Methylene-Bis-Acrylamide, 0.25 g, with functionality two. The photoinitiator system consists of triethanolamine, 2mL, acting as an electron acceptor, and yellowish eosin, 0.7 ml (0.8% w/v), acting as an electron donor. The latter is highly absorptive at a recording wavelength of 532 nm but has no absorption at a light guiding wavelength of 632.8 nm.

The thiol-ene based NPC system consisted of the stoichiometric mixture of thiol-ene monomer, containing allyl triazine ene monomer, triallyl-1,3,5-triazine-2,4,6(1H,3H,5H)-trione (Aldrich), and dithiol monomer, 1,4-bis(3-mercaptobutyryloxy) butane (Aldrich). SiO_2 nanoparticles (the average size of 13 nm), dissolved in methyl isobutyl ketone (MIBK) at a concentration of 30 wt. % were used for their dispersion in the thiol-ene monomer blend [20–22]. The refractive index difference between SiO_2 nanoparticles and the formed thiol-ene polymer is close to 0.1, which helps to obtain large values of the refractive index modulation. The dispersion of nanoparticles also improves the thermal stability of the gratings recorded in the NPC material, as reported earlier [21,23]. The efficient polymerization of the thiol-ene NPC material by a green laser was achieved by the addition of 2 wt. % of titanocene organo-metallic complex (Chivacure 534, Chitec Tech.) in combination with 2.5 wt. % benzoyl peroxide (BzO2, Aldrich). The mixed syrup was dripped on a glass substrate and dried in an oven at 55° C for 20 minutes to eliminate the MIBK solvent. Then, another glass substrate was placed to cover the dipped syrup. We used 20-30 μm glass microspheres as spacers between the two glass substrates.

The last material analyzed is PDLC. The monomer used was dipentaerythritol penta-/hexaacrylate (DPHPA), with a refractive index n = 1.490. We used the nematic liquid crystal BL036 from Merck. It is a mixture of 4-cyanobiphenyls with alkyl chains of different lengths. It has an ordinary refractive index n_0 = 1.5270 and a difference between extraordinary and ordinary index Δn = 0.2670 [24]. The liquid crystal concentration was set at 28 wt% as the starting point for component optimization and remained practically unchanged during this process. N-vinyl-2-pyrrolidone (NVP) was used as crosslinker, N-phenylglicine (NPG) as radical generator, octanoic acid (OA) as cosolvent [24] and ethyl eosin (YEt) as dye. N-methyl-2- pyrrolidone was used in combination with NVP in order to control overmodulation during hologram recording [24]. The prepolymer solution was made by mixing the components under red light to which the material is not sensitive. The solution was sonicated in an ultrasonic bath, deposited between glass plates 1mm thick, separated using glass microspheres as spacers. The microspheres were provided by Whitehouse Scientific with a thickness between 20 and 30 μm.

4. Results and discussion

In this section, we analyze three types of photopolymers for this waveguide application [17]. To be sure that the particular chemical compositions are able to support these waveguides and have enough resolution, we compare the material response with symmetrical gratings for three different spatial frequencies: 1000, 1700 and 2000 lines/mm. After this analysis, we compare the material behavior for the fabrication of the different geometries of waveguides proposed. Firstly, we study PVA/AA material. The second material analyzed, thiol-ene NPC, was firstly studied in [21–23]. With its higher value of monomer functionality, we expected more physical support for the slanted gratings recorded. On the third place, we analyzed, PDLC, a multifunctional monomer with functionality higher than 5. Finally, the results

obtained by the three materials are compared and the ways to improve their behavior is discussed based on the results obtained by the three geometrical recording architectures.

PVA/AA material

As we mentioned in the introduction, PVA/AA materials have been evaluated for many different applications related to holography and diffractive elements. We know that the refractive index modulation of acrylamide systems begins to decrease for spatial frequencies higher than 1500 lines/mm [27] and for 2000 lines/mm this value drops to 70%. Therefore, the highest value of diffraction efficiency, DE, achieved for the recording geometry proposed in Fig. 2, was about 20% in the preliminary studies using recording geometry A [18]. This value contrasts with the good behavior exhibited by the same composition for unslanted gratings at the spatial frequency of 2000 lines/mm [17,27]. That means that something happens when tilted gratings are stored in the material. Maybe the material suffers important deformations when non-symmetric structures with low grating spacing are recorded on it. In order to avoid this phenomenon, we have introduced the index matching system proposed in [28] for low spatial frequency DOEs fabrication, but the results are similar. In Fig. 3, we present the recording of symmetrical gratings for three layers, 70 µm thick, for three different spatial frequencies: 1000 lines/mm, 1700 lines/mm and 2000 lines/mm. The diffraction efficiency is not corrected taking into account the Fresnel losses for TE incidence. Therefore, the theoretical maximum value of the DE is around 90%, which means that 90% of the incident power can be diffracted, indicating that TE is nearly 0%. As it can be seen in Fig. 3, the HOE with PVA/AA material presents better behavior at the spatial frequency of 1000 lines/mm, since the refractive index modulation achieved is the largest in this case. Nevertheless, it can be seen how the length of the polymer chains affects at high spatial frequencies increasing the time to achieve TE around 0% (i.e. maximum DE) and reducing the refractive index modulation stored as was observed in PVA/AA [29] also in other materials [30].

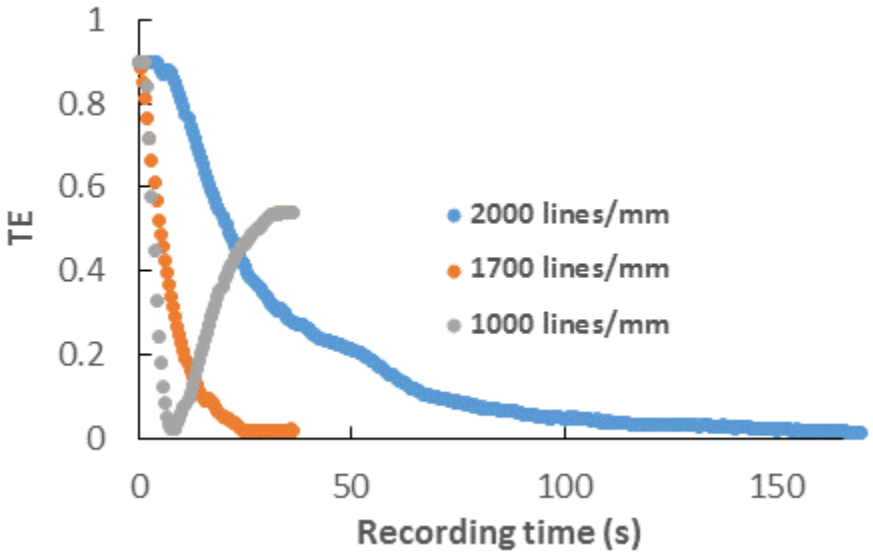

Fig. 3. TE as a function of the recording time for unslanted gratings for different spatial frequencies recorded in PVA/AA photopolymer.

Once we checked that the PVA/AA has enough resolution to record the required gratings, we need to analyze the behavior for slanted proposed geometries. In this case we have found that the DE achieved is clearly smaller than the ones obtained for unslanted gratings with the

Optics EXPRESS

similar DE. These values can be seen in Fig. 4 where the angular scan about the first Bragg angle is represented. We compare the behavior for geometries A and B, different recording schemes in this material analyzing the angular responses of the recorded waveguides. In these figures the transmission efficiency, TE, is represented as a function of the readout angle. Therefore, we have represented the TE as function of the readout angle in air. It is important to note that for both geometries the Bragg angle changes. In the geometry A, Fig. 4(a), the Bragg angle is close to the normal and in the geometry B, Fig. 4(b), is few degrees deviated from this, for the readout wavelength of 632 nm. As it can be seen also in Fig. 4, PVA/AA material presents moderate better behavior for geometry type B, where the fringes are less slanted. In this case, we can guide about the half of the beam energy into our material, and with previously proposed geometry A, around 33%. The experimental angular response was fitted using Kogelnik's coupled wave theory [31], KCW, to determine the optical thickness, d, refractive index modulation, n_1, and the coefficient of absorption and scattering, α, for the recorded holograms. The data for Fig. 4(a), with spatial frequency of 2000 lines/mm, are d = 64 μm, $n_1 = 0.00190$ and $\alpha = 0.003\ \mu m^{-1}$. And for Fig. 4(b) d = 68 μm, $n_1 = 0.00235$ and $\alpha = 0.003\ \mu m^{-1}$.

It is worth noting that for the angular responses at more slanted gratings some irregularities appear in comparison to geometry B. Nevertheless, it is important to say that the repeatability on the results in both cases is not as high as in the case of symmetric gratings. This is an important drawback for this material in order to use it for this application. It can be due to the shrinkage during the grating formation and the soft consistence of the polymer chains. In order to solve this point, we can evaluate multifunctional polymers to achieve polymer structures with more physical support for waveguide application. In Fig. 4(c) we show a photograph of the waveguide recorded in geometry B at a probe wavelength of 633 nm. It can be seen that a large amount of the incident beam is trapped inside the glass substrate and guided to its edge, where the incidence angle is smaller than the critical one, and therefore can be refracted to the air.

Optics EXPRESS

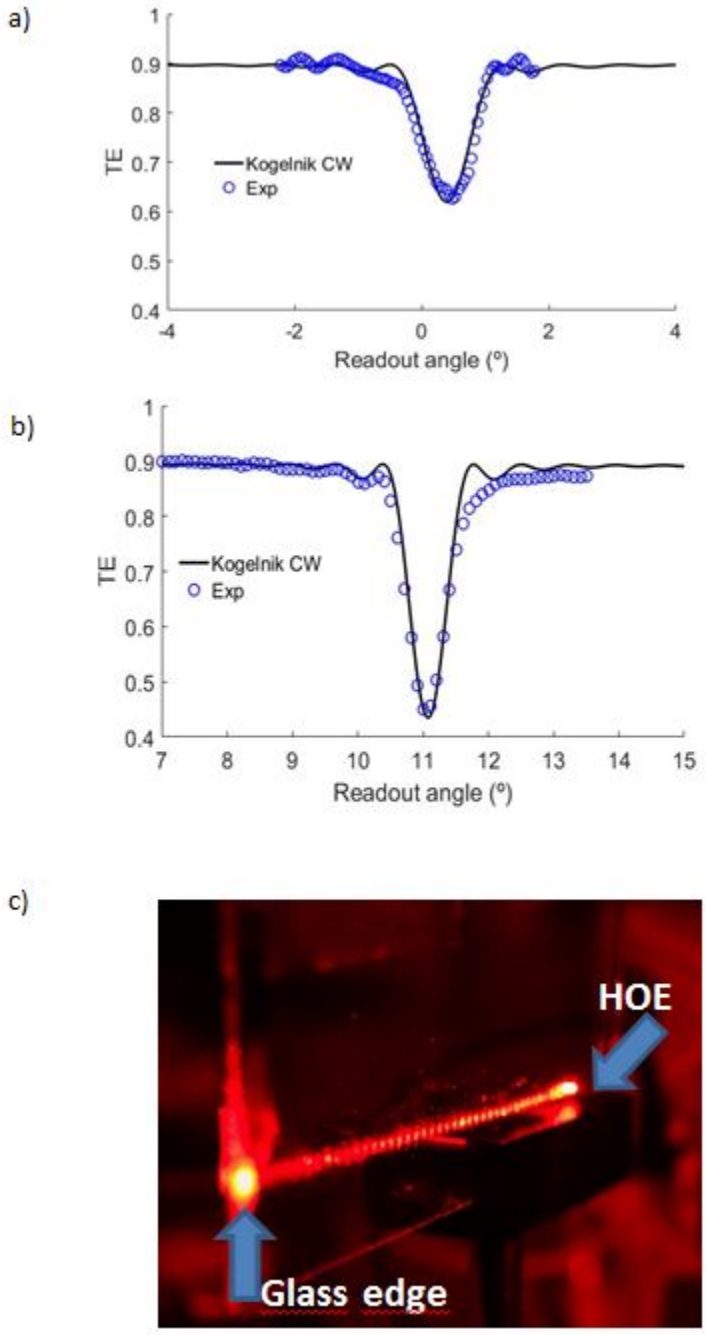

Fig. 4. Angular responses of the grating-coupler recorded at PVA/AA material. a) Geometry A, TE as function of the incidence angle in air b) Geometry B, TE as function of the incidence angle in air c) Image of the waveguide using Geometry B at readout 633 nm.

NPC material

Previous studies reported the properties of thiol-ene NPC gratings recorded at spatial frequencies lower than 2500 mm/lines (grating spacing larger than 0.4 μm) with substantive shrinkage suppression as a result of SiO_2 dispersion [22,23]. The results for a spatial

Optics EXPRESS

frequency dependence of DE investigated in this work are presented in Fig. 5 for thiol-ene NPC symmetrical gratings with thickness around 21 μm. In comparison with that of the PVA/AA material, we observed noticeable results of thiol-ene NPC gratings recorded at higher spatial frequencies. As seen in Fig. 5, the values for TE at spatial frequencies higher than 1000 lines/mm decrease slightly. We attribute this trend to our use of a recording intensity lower than 5 mW/cm^2 at which higher DEs (~60%) were obtained with the ~15-μm thick thiol-ene NPC grating [21] as a result of shorter polymer chain formation at higher recording intensities during holographic recording [19]. In [21] DEs of 60% were achieved with gratings with thickness around 15 μm. We suggest that one way to increase DEs at high spatial frequencies is to use a thicker NPC film without significant holographic scattering. An additional option is to study architectures for this kind of waveguides where the high spatial frequency requirement can be relaxed. Nevertheless, as can be found in the theoretical background section, the grating should be largely slanted so that one of incident angles of two recording beams is more oblique, which requires the use of prisms in the experimental set-up.

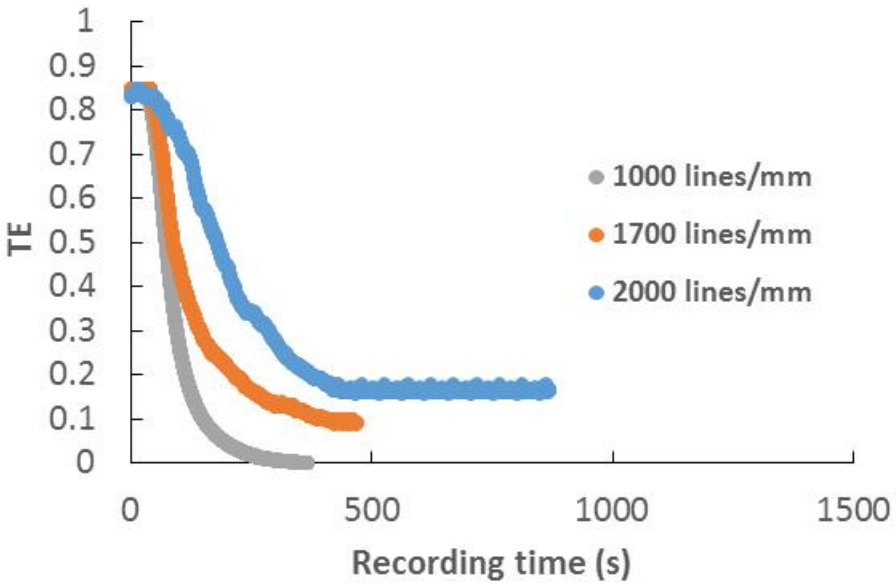

Fig. 5. TE as a function of the recording time for symmetric gratings for different spatial frequencies recorded in the thiol-ene based NPC material of 21 μm thickness.

From the measured Bragg-angle detuning dependences of TEs presented in Fig. 6 and data fitting using KCW, looking at the secondary lobes in the angular responses it can be seen that the data are symmetric as compared with the ones observed in PVA/AA material. That indicates that the grating distortion caused by shrinkage is much smaller with the thiol-ene based NPC material than that with the PVA/AA material. It can also be seen that when comparing with PVA/AA materials, the width of the Bragg-detuning curve is wider due to the thickness of the thiol-ene NPC films, which is thinner than that of the PVA/AA material. The width of the central lobe is related to the angular selectivity of the recorded grating. For the two cases depicted in Figs. 6(a) and 6(b), the fitted values for these gratings are d = 24 μm, n_1 = 0.0092 and α = 0.001 μm^{-1} for Fig. 6(a) and d = 18 μm, n_1 = 0.0090 and α = 0.002 μm^{-1} for Fig. 6(b). As we can see, values for n_1 shown above are similar and clearly larger than the ones obtained for PVA/AA material as shown in Fig. 4. More than 50% of light can be trapped and guided by the display, with a thiol-ene NPC thin film of the order of 20 μm. Furthermore, it can be found that the geometry C (Fig. 6(c)) provides d = 19 μm, n_1 = 0.011 and α = 0.002 μm^{-1}. In this geometry TE is only 20%, the main percentage of light is guided

Optics EXPRESS

into the glass. That means that the thiol-ene based NPC material can record a slanted grating with large n_1 at low spatial frequencies. It is important to note that the ripple observed out of Bragg angle for the geometry B (Fig. 6(b)), is caused by the multiple reflection between two glass substrates. It is also important to note that the largest value of DE is achieved for the geometry C among the three geometries A, B and C. DE is still 10% smaller than the one obtained for symmetric recording, non-slanted gratings [23]. In the case of non-slanted gratings DE can be 100% with this thickness as shown in Fig. 5.

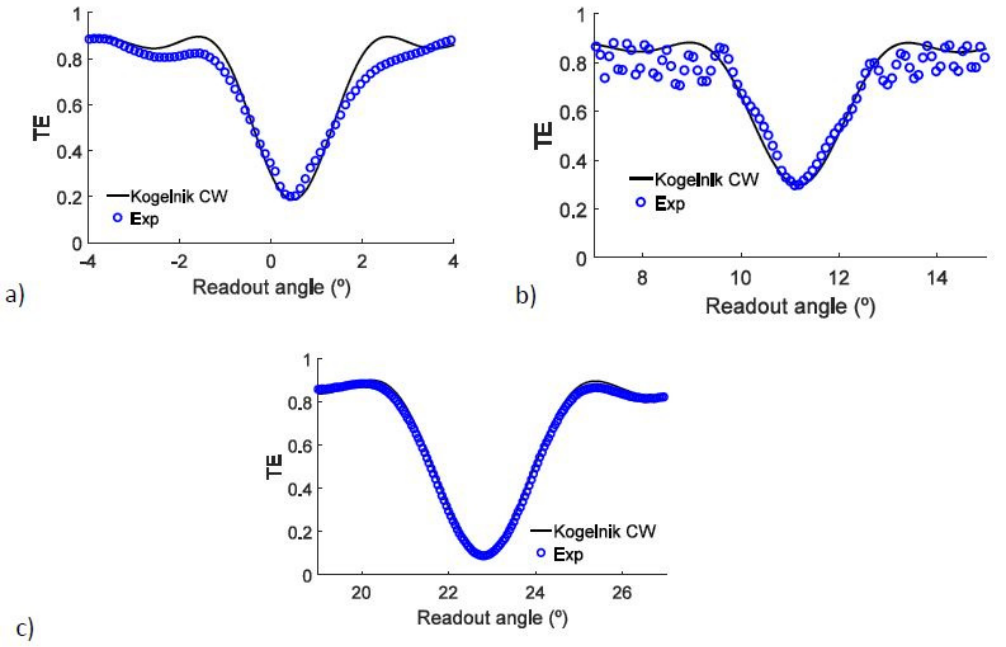

Fig. 6. Bragg-detuning curves for NPC materials with a) the geometry A, b) the geometry B and c) the geometry C at readout 632 nm.

PDLC material

As an alternative to the two photopolymers previously studied, we have developed a similar analysis using PLC material. This material presents good behavior for symmetric gratings with spatial frequencies around 1000 lines/mm for different thicknesses [32], and a functionality between 5 and 6. This high value of functionality is recommended in order to produce a phase separation between polymer and liquid crystal molecules during polymerization, concentrating the liquid crystal molecules in the less illuminated zones during recording. Furthermore, that confers the possibility to manufacture tunable holographic optical elements. This material presents high support for slanted geometry and the DE are quite similar for symmetric and slanted geometry. Therefore, we have depicted the evolution of the transmission efficiency, TE, as a function of recording time in Fig. 7, for both architectures in the registration step. As we can see, this material presents good energetic sensitivity, close to PVA/AA materials. In this case, the gratings recorded with geometry A have 35 μm thickness and the values fitted of refractive index modulation and scattering coefficient were $n_1 = 0.0060$ and $\alpha = 0.0041$ μm^{-1}. In the case of recording geometry B, 2000 lines/mm, the optical thickness of the sample was 40 μm, $n_1 = 0.0055$ and $\alpha = 0.0049$ μm^{-1}. That means that this kind of material can be used for high spatial frequencies with promising results, as the decrease of the refractive index modulation is less than 10%. In both cases, the light captured was higher than 70%, and in the case of geometry A, around 80%. These

Optics EXPRESS

percentages can be obtained with layers of thickness between 30 and 40 µm. Due to the good results with geometries A and B for PDLC is not necessary to try geometry C.

It is possible to eliminate the transmitted beam, with efficiencies close to 0% if we use thicker samples. As an example, we show Fig. 8(a), where a grating with thickness around 50 µm recorded with geometry A is presented, it can be seen that even this grating is slightly overmodulated. As it can be seen, around 98% of the light can be guided at Bragg's condition. In general, for PDLC systems the value of refractive index modulation, n_1, is a tensor and depends on the polarization state [33]. In our experiments the angular response is made by TE polarization, *s* polarization, one of the neutral lines of the HOE, therefore, KCW can be applied. The values fitted for this grating using KCW were d = 54 µm, $n_1 = 0.0063$ and $\alpha = 0.007\ \mu m^{-1}$. As we can see, the scattering coefficient is high in comparison with previous results. It makes sense because the chemical composition does not change and the thickness is higher [32]. With thinner layers also higher refractive index modulations can be achieved, around $1.2\ 10^{-2}$ [32]. To have a deeper insight of the behavior of this wave-coupler, it can be tested using white light or solar light. Then it can be seen how the selected wavelength, in our case the red ones, is guided along the glass substrate while the other ones are reflected or transmitted. This effect can be seen clearly when the HOE presents high DE. Figure 8(b), shows a diagram of the behavior of the HOE with solar light and in Fig. 8(c) we present the experiment. It can be seen how the longest wavelengths are guided by the substrate and the shortest ones do not. This wave-coupler can be designed to trap the desired part of the spectrum; therefore, new applications can be opened using this system.

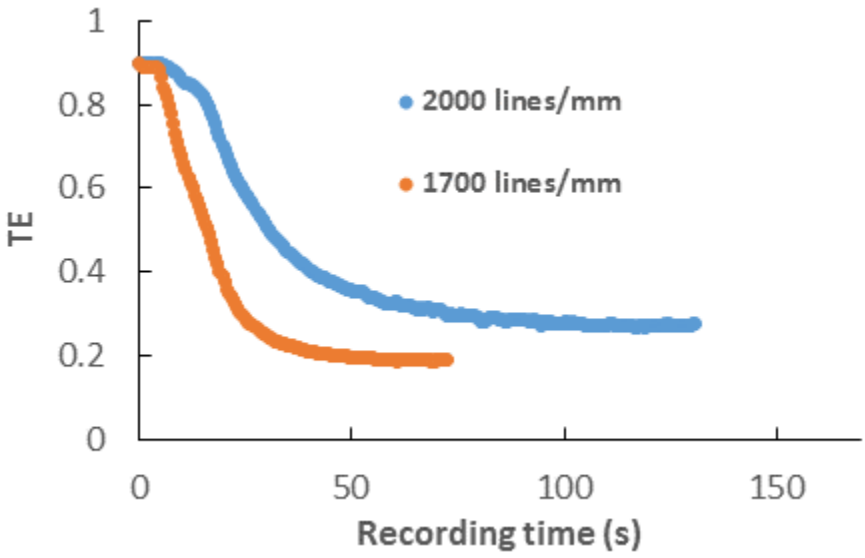

Fig. 7. TE as a function of the recording time for the waveguide for geometry A, 1700 lines/mm and geometry B, 2000 lines/mm, for PLC photopolymer layers 35-39 µm thick.

Optics EXPRESS

a)

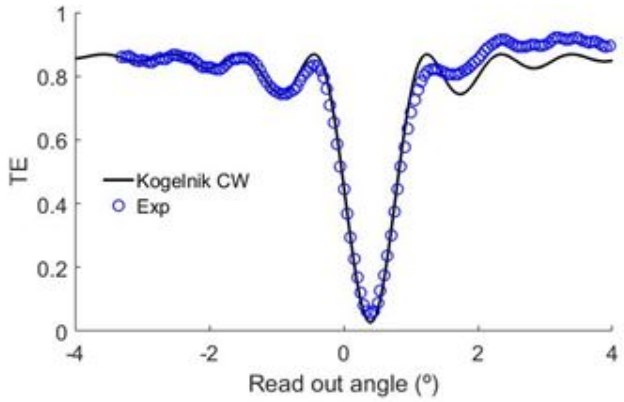

b)

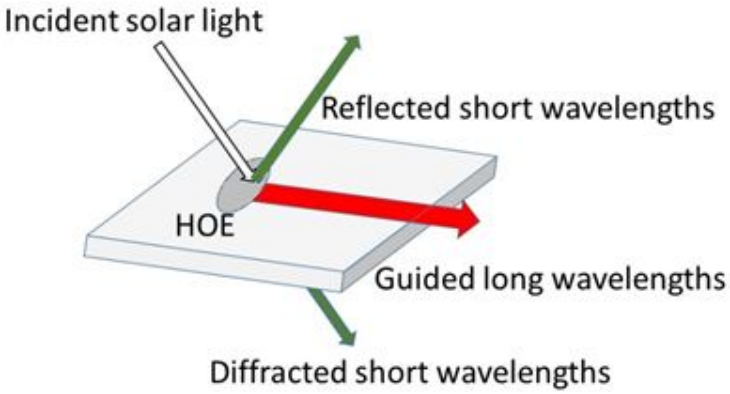

c)

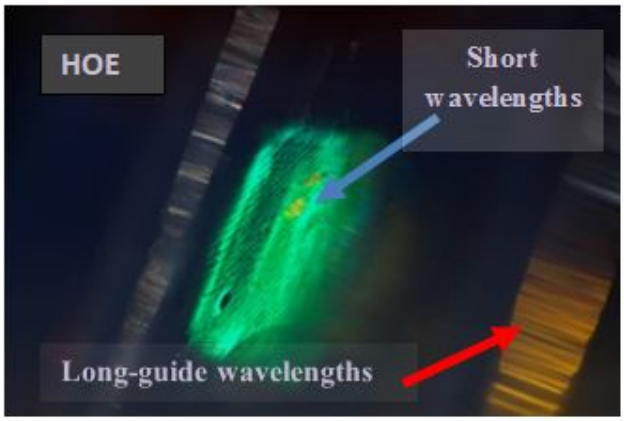

Fig. 8. a) Angular response of an overmodulated waveguide recorded in PDLC material using geometry A with thickness of 54 µm. b) Diagram of the HOE behavior under solar light. c) Image of the HOE under normal sun light.

Optics EXPRESS

5. Conclusions

To summarize, we have evaluated the fabrication of waveguides in three different photopolymers using three different geometries. In all of them, the display can be recorded with interesting percentage of incident light guided through the substrate, but for the PVA/AA and NPC, the DE is limited for different reasons in each case. For PVA/AA material, the lack of physical support during the recording of the slanted gratings prevents the optimal recording. Nevertheless, it has good spatial resolution of 2000 lines/mm. Thiol-ene based NPC with the monomer functionality between 2 and 3 supports the slanted geometry better and exhibits relatively low resolution limitation: the refractive index modulation drops by 20% at spatial frequencies higher than 1000 lines/mm at recording intensities used. High percentages of guided light can be obtained more easily by geometry C provided that the sample layer is 20 μm or thicker. Optimum results are obtained for PDLC material. In this case, we can achieve the maximum DE with thickness lower than 60 μm with energetic sensitivity close to the one of PVA/AA materials and low scattering. It is worth noting that, depending on the material, it is important to properly choose the optimum recording geometry. It is possible to guide the light using transmission holographic elements with different spatial frequencies and slanted angles. Despite this, applications of see-through glasses, where high DE are not required, are suitable in the three materials studied. Depending on the concrete application and the importance of the angular selectivity or energetic sensitivity, we can choose PVA/AA or NPC.

Funding

"Ministerio de Economía Industria y Competitividad" (Spain) under projects FIS2017-82919-R (MINECO/AEI/FEDER, UE) and FIS2015-66570-P (MINECO/FEDER); "Generalitat Valenciana" (Spain) (PROMETEOII/2015/015). R. F. and Y. T., acknowledge a financial support by the Ministry of Education, Culture, Sports, Science and Technology of Japan under grant 15H03576.

References

1. H. J. Coufal, D. Psaltis, and G. T. Sincerbox, eds., *Holographic Data Storage*; (Springer–Verlag, 2000).
2. M. Infusino, A. De Luca, V. Barna, R. Caputo, and C. Umeton, "Periodic and aperiodic liquid crystal-polymer composite structures realized via spatial light modulator direct holography," Opt. Express **20**(21), 23138–23143 (2012).
3. R. Fernández, S. Gallego, A. Márquez, J. Francés, V. Navarro-Fuster, and I. Pascual, "Diffractive lenses recorded in absorbent photopolymers," Opt. Express **24**(2), 1559–1572 (2016).
4. J. M. Miller, N. de Beaucoudrey, P. Chavel, J. Turunen, and E. Cambril, "Design and fabrication of binary slanted surface-relief gratings for a planar optical interconnection," Appl. Opt. **36**(23), 5717–5727 (1997).
5. M. Miki, R. Ohira, and Y. Tomita, "Optical properties of electrically tunable two-dimensional photonic lattice structures formed in a holographic polymer-dispersed liquid crystal film: analysis and experiment," Materials (Basel) **7**(5), 3677–3698 (2014).
6. K. Curtis, L. Dhar, A. Hill, W. Wilson, and M. Ayres, eds., *Holographic Data Storage: From Theory to Practical Systems* (John Wiley & Sons, Ltd., 2010).
7. E. Leite, I. Naydenova, S. Mintova, L. Leclercq, and V. Toal, "Photopolymerizable nanocomposites for holographic recording and sensor application," Appl. Opt. **49**(19), 3652–3660 (2010).
8. I. Naydenova, H. Akbari, C. Dalton, M. Y. M. Ilyas, C. P. T. Wei, V. Toal, and S. Martin, Photopolymer Holographic Optical Elements for Application in Solar Energy Concentrators, Holography - Basic principles and contemporary applications, Dr. Emilia Mihaylova (Ed., InTech, 2013).
9. J. Y. Hong, C.-K. Lee, S. Lee, B. Lee, D. Yoo, C. Jang, J. Kim, J. Jeong, and B. Lee, "See-through optical combiner for augmented reality head-mounted display: index-matched anisotropic crystal lens," Sci. Rep. **7**(1), 2753 (2017).
10. E. Tolstik, O. Romanov, V. Matusevich, A. Tolstik, and R. Kowarschik, "Formation of self-trapping waveguides in bulk PMMA media doped with Phenanthrenequinone," Opt. Express **22**(3), 3228–3233 (2014).
11. H. Li, Y. Qi, J. P. Ryle, and J. T. Sheridan, "Self-written waveguides in a dry acrylamide/polyvinyl alcohol photopolymer material," Appl. Opt. **53**(34), 8086–8094 (2014).
12. J. Marín-Sáez, J. Atencia, D. Chemisana, and M.-V. Collados, "Characterization of volume holographic optical elements recorded in Bayfol HX photopolymer for solar photovoltaic applications," Opt. Express **24**(6), A720–A730 (2016).

Optics EXPRESS

13. J. Guo, M. R. Gleeson, and J. T. Sheridan, "A review of the optimisation of photopolymer materials for holographic data storage," Physics Research International **2012**, 803439 (2012).
14. G. Li, D. Lee, Y. Jeong, J. Cho, and B. Lee, "Holographic display for see-through augmented reality using mirror-lens holographic optical element," Opt. Lett. **41**(11), 2486–2489 (2016).
15. N. Zhang, J. Liu, J. Han, X. Li, F. Yang, X. Wang, B. Hu, and Y. Wang, "Improved holographic waveguide display system," Appl. Opt. **54**(12), 3645–3649 (2015).
16. J. A. Piao, G. Li, M. Lan Piao, and N. Kim, "Full Color Holographic Optical Element Fabrication for Waveguide-type Head Mounted Display Using Photopolymer," J. Opt. Soc. Korea **17**(3), 242–248 (2013).
17. C. Neipp, J. Francés, F. J. Martínez, R. Fernández, M. L. Alvarez, S. Bleda, M. Ortuño, and S. Gallego, "Optimization of Photopolymer Materials for the Fabrication of a Holographic Waveguide," Polymers (Basel) **9**(9), 395 (2017).
18. J. T. Sheridan and J. R. Lawrence, "Nonlocal-response diffusion model of holographic recording in photopolymer," J. Opt. Soc. Am. A **17**(6), 1108–1114 (2000).
19. M. R. Gleeson, D. Sabol, S. Liu, C. E. Close, J. V. Kelly, and J. T. Sheridan, "Improvement of the spatial frequency response of photopolymer materials by modifying polymer chain length," J. Opt. Soc. Am. B **25**(3), 396–406 (2008).
20. R. Fernández, S. Gallego, V. Navarro-Fuster, C. Neipp, J. Francés, S. Fenoll, I. Pascual, and A. Beléndez, "Dimensional changes in slanted diffraction gratings recorded in photopolymers," Opt. Mater. Express **6**(11), 3455–3468 (2016).
21. E. Hata and Y. Tomita, "Order-of-magnitude polymerization-shrinkage suppression of volume gratings recorded in nanoparticle-polymer composites," Opt. Lett. **35**(3), 396–398 (2010).
22. E. Hata, K. Mitsube, K. Momose, and Y. Tomita, "Holographic nanoparticle-polymer composites based on step-growth thiol-ene photopolymerization," Opt. Mater. Express **1**(2), 207–222 (2011).
23. E. Hata and Y. Tomita, "Stoichiometric thiol-to-ene ratio dependences of refractive index modulation and shrinkage of volume gratings recorded in photopolymerizable nanoparticle-polymer composites based onstep-growth polymerization," Opt. Mater. Express **1**(6), 1113–1120 (2011).
24. M. Ortuño, M. Riquelme, S. Gallego, A. Márquez, I. Pascual, and A. Beléndez, "Overmodulation control in the optimization of a H-PDLC device with ethyl eosin as dye," International Journal of Polymer Science **2013**, 357963 (2013).
25. C. Meka, R. Jallapuram, I. Naydenova, S. Martin, and V. Toal, "Development of a panchromatic acrylamide-based photopolymer for multicolor reflection holography," Appl. Opt. **49**(8), 1400–1405 (2010).
26. D. Yu, H. Liu, D. Mao, Y. Geng, W. Wang, L. Sun, and J. Lv, "Enhancement of spectrum strength in holographic sensing in nanozeolites dispersed acrylamide photopolymer," Opt. Express **23**(22), 29113–29126 (2015).
27. F. T. O'Neill, J. R. Lawrence, and J. T. Sheridan, "Thickness variation of self-processing acrylamide-based photopolymer and reflection holography," Opt. Eng. **40**(4), 533–539 (2001).
28. S. Gallego, R. Fernández, A. Márquez, M. Ortuño, C. Neipp, M. R. Gleeson, J. T. Sheridan, and A. Beléndez, "Two diffusion photopolymer for sharp diffractive optical elements recording," Opt. Lett. **40**(14), 3221–3224 (2015).
29. M. Moothanchery, I. Naydenova, and V. Toal, "Studies of shrinkage as a result of holographic recording in acrylamide-basedphotopolymer film," Appl. Phys., A Mater. Sci. Process. **104**(3), 899–902 (2011).
30. F.-K. Bruder, T. Fäcke, and T. Rölle, "The Chemistry and Physics of Bayfol HX Film holographic Photopolymer," Polymers (Basel) **9**(12), 472 (2017).
31. H. Kogelnik, "Coupled wave theory for thick hologram gratings," Bell Labs Tech. J. **48**(9), 2909–2947 (1969).
32. S. Gallego, M. Ortuño, A. Márquez, R. Fernández, M. Álvarez, I. Pascual, and A. Beléndez, "Influence of thickness on the holographic parameters of h-pdlc materials," Int. J. Polym. Sci. **2014**, 528287 (2014).
33. M. Jazbinšek, I. Drevensek-Olenik, M. Zgonik, A. K. Fontecchio, and G. P. Crawford, "Characterization of holographic polymer dispersed liquid crystal transmission gratings," J. Appl. Phys. **90**(8), 3831–3837 (2001).